

Reflection and transmission of an Airy beam in a dielectric slab

Xiaojin Yang(杨小锦), Tan Qu(屈檀), Zhensen Wu(吴振森), Haiying Li(李海英), Lu Bai(白璐), Lei Gong(巩蕾), and Zhengjun Li(李正军)

Citation: Chin. Phys. B, 2022, 31 (**7**): 074202. DOI: 10.1088/1674-1056/ac4e07
Journal homepage: http://cpb.iphy.ac.cn; http://iopscience.iop.org/cpb

What follows is a list of articles you may be interested in

Nonparaxial propagation of radially polarized chirped Airy beams in uniaxial crystal orthogonal to the optical axis

Yaohui Chen(陈耀辉), Lixun Wu(吴理汛), Zhixiong Mo(莫智雄), Lican Wu(吴利灿), and Dongmei Deng(邓冬梅)
Chin. Phys. B, 2021, 30 (**1**): 014204. DOI: 10.1088/1674-1056/abb226

Hyperbolic metamaterials for high-efficiency generation of circularly polarized Airy beams

Lin Chen(陈林), Huihui Li(李会会), Weiming Hao(郝玮鸣), Xiang Yin(殷祥), Jian Wang(王健)
Chin. Phys. B, 2020, 29 (**8**): 084210. DOI: 10.1088/1674-1056/ab96a1

Three-Airy autofocusing beams

Xiao-Hong Zhang(张小红), Fei-Li Wang(王飞利), Lu-Yang Bai(白露阳), Ci-Bo Lou(楼慈波), Yi Liang(梁毅)
Chin. Phys. B, 2020, 29 (**6**): 064204. DOI: 10.1088/1674-1056/ab84d2

Dynamics of Airy beams in parity-time symmetric optical lattices

Rui-Hong Chen(陈睿弘), Wei-Yi Hong(洪伟毅)
Chin. Phys. B, 2019, 28 (**5**): 054202. DOI: 10.1088/1674-1056/28/5/054202

Relation between Airy beams and triple-cusp beams

Ren Zhi-Jun, Li Xiao-Dong, Jin Hong-Zhen, Chen Chen, Wu Jiang-Miao
Chin. Phys. B, 2014, 23 (**8**): 084202. DOI: 10.1088/1674-1056/23/8/084202

Reflection and transmission of an Airy beam in a dielectric slab

Xiaojin Yang(杨小锦)[1], Tan Qu(屈檀)[2,†], Zhensen Wu(吴振森)[1], Haiying Li(李海英)[1], Lu Bai(白璐)[1], Lei Gong(巩蕾)[3], and Zhengjun Li(李正军)[1]

[1] *School of Physics and Optoelectronic Engineering, Xidian University, Xi'an* 710071, *China*
[2] *School of Electronic Engineering, Xidian University, Xi'an* 710071, *China*
[3] *School of Photoelectric Engineering, Xi'an Technological University, Xi'an* 710021, *China*

(Received 26 October 2021; revised manuscript received 15 January 2022; accepted manuscript online 24 January 2022)

The reflection and transmission of a finite-power Airy beam incident on a dielectric slab are investigated by an analytical method. Based on the plane-wave angular spectrum expansion and Fresnel approximation, the analytical expressions of the reflected field, internal field as well as transmitted field in each region are obtained. Through numerical simulations, the intensity distributions of the incident beam, reflected beam, internal beam as well as transmitted beam are presented at oblique incidence. Besides, we also compare the intensity distributions of the geometrical-optics beam field, the first order beam mode field and the actual beam field, which indicates that the contribution of each order beam mode field to the actual beam field is related to the refractive index of the dielectric slab. Meanwhile, the reflection characteristics of the Airy beams in the special cases of Brewster incidence and total reflection are investigated. Finally, the effects of the optical thickness and refractive index of the dielectric slab on the peak intensity distributions and beam shifts of the reflected and transmitted beams are also discussed in detail. The analytical and numerical results will be useful to analyze the propagation dynamics of Airy beam in the dielectric slab and provide some theoretical supports to the design of optical film.

Keywords: Airy beam, dielectric slab, Fresnel approximation, reflection and transmission

PACS: 42.25.Bs, 42.60.Jf, 42.25.Gy **DOI:** 10.1088/1674-1056/ac4e07

1. Introduction

The Airy beam was firstly predicted by Berry and Balazs as a solution to potential-free Schrödinger's equation in quantum mechanics.[1] It was not until 2007 that the finite energy Airy beam was realized theoretically and experimentally by Siviloglou and Christodoulides.[2,3] Recently, nondiffracting[4] and self-accelerating[2,3] Airy beam has attracted a great deal of interest due to its intriguing properties and potential applications[5,6] such as in optical micromanipulation,[7–9] curved plasma channel generation,[10,11] vacuum electron acceleration,[12,13] surface plasmon polariton[14–17] and imaging transmission.[18–20]

The interaction of Airy beams with different media is becoming a hot spot in these days. As is well known, the reflected and transmitted fields of a plane wave are described by Snell's law and Fresnel formulas,[21] which provides the geometrical-optics field of the beam. However, for a bounded light beam, Snell's law and Fresnel formulas are no longer active and the nonspecular phenomena such as Goos–Hänchen (GH) and Imbert–Fedorov (IF) shifts occur.[22–24] The GH and IF shifts of various beams, including Gaussian beams,[25] rotating elliptical Gaussian beams,[26,27] elegant Hermite–Gaussian beams[28] and spin waves,[29] incident on different types of surfaces[30] have been studied. The effects of different media on bounded beams are discussed by several methods. Employing the plane-wave angular spectrum expansion and Fresnel approximation, Tamir[31] and Antar[32] studied the reflection and transmission of a Gaussian beam in a planar dielectric interface, and Okuda[33] and Ou[34] discussed the interaction of Laguerre–Gaussian beam with a dielectric interface theoretically and experimentally. In the same way, Li further studied the reflection and transmission of Laguerre–Gaussian beam in a dielectric slab[35] and uniaxial anisotropic multilayered media.[36] Meanwhile, Li also used this method to analyze the propagation characteristics of a vector Bessel vortex beam through multilayered isotropic media.[37] Based on the generalized Lorenz–Mie theory (GLMT), Wang and Yan studied separately the reflection and transmission of a Gaussian beam in a uniaxial anisotropic slab[38] and a chiral slab[39] by a combination of the cylindrical vector wave functions expansion of beams and boundary conditions. Li also used this method to analyze the reflection and transmission of a Bessel vortex beam incident on a homogeneous[40,41] and stratified uniaxial anisotropic slab,[42] respectively.

For the case of Airy beams, Efremidis firstly studied the refraction and reflection of a finite-power Airy beam from a dielectric interface at Brewster and total internal reflection angles,[43] and then he further studied the reflection and transmission dynamics of an Airy beam impinging on refractive index potentials.[44] The selective reflection of an Airy beam at an interface was also reported.[45] Pedro numerically studied the giant Goos–Hänchen shifts of Airy beams impinging on a nonlinear interface based on the nonlinear Helmholtz equation.[46] The Goos–Hänchen and Imbert–Fedorov shifts

†Corresponding author. E-mail: tqu@xidian.edu.cn

© 2022 Chinese Physical Society and IOP Publishing Ltd

of different kinds of Airy beams impinging on various dielectric surface were presented based on the angular spectrum expansion.[47–50] Although some research on the interaction of Airy beams with dielectric interface have been studied in detail, the beam field characteristics of an Airy beam impinging on a dielectric slab, such as the beam field intensity distributions, the contribution of each order beam mode field to the actual beam field, and the influence of the dielectric slab parameters, have not been reported systematically, which is the purpose of this work.

In this paper, the reflection and transmission of a finite-power Airy beam through a dielectric slab are investigated analytically. Based on the plane-wave angular spectrum expansion, the analytical expressions of the incident field, reflected field, internal field and transmitted field for a paraxial Airy beam incident in a dielectric slab are derived in Section 2. The intensity distributions of the incident beam, reflected beam, internal beam as well as transmitted beam are simulated, and the discussion of the effects of the optical thickness and refractive index of the dielectric slab on the peak intensity distributions and beam shifts of the reflected and transmitted beams is also given in Section 3. Finally, the paper is concluded in Section 4.

2. Theoretical formulation

It is shown the geometry of coordinate system for the reflection and transmission of an Airy beam impinging on a dielectric slab in Fig. 1. The input and output regions are infinite half spaces, and the refractive index, dielectric constant and wave number in each region are n_β, ε_β and k_β, respectively, where $\beta = 1,2,3$. The relative magnetic susceptibility of each region is assumed to be unity. The thickness of the slab is d. For the sake of simplicity and in order to focus on the essentials, we assume a 2D variation $(\partial/\partial y = 0)$. The global coordinate system (x,z) is situated on the first interface $(z=0)$, and the three local coordinates for incident, reflected, and transmitted beams are referred to as (x_α, z_α), $\alpha = \{\mathrm{i},\mathrm{r},\mathrm{t}\}$. The angle between the z_i and z axis is defined as incident angle θ_i. Similarly, the reflection angle and transmission angle are described as $\theta_\mathrm{r} = \pi - \theta_\mathrm{i}$ and θ_t. θ_2 is the refracted angle of the beam in the dielectric slab.

The origins of the coordinates $(x_\mathrm{i}, z_\mathrm{i})$, $(x_\mathrm{r}, z_\mathrm{r})$, $(x_\mathrm{t}, z_\mathrm{t})$ are located at $(-s,-h)$, $(-s,h)$ and $(-(s-l),-h')$, respectively, where $s = h\tan\theta_\mathrm{i}$. The transformations between the coordinates $(x_\mathrm{i}, z_\mathrm{i})$, $(x_\mathrm{r}, z_\mathrm{r})$, $(x_\mathrm{t}, z_\mathrm{t})$ and the global coordinate (x,z) are described as

$$\begin{aligned} x_\mathrm{i} &= (x+s)\cos\theta_\mathrm{i} - (z+h)\sin\theta_\mathrm{i}, \\ z_\mathrm{i} &= (x+s)\sin\theta_\mathrm{i} + (z+h)\cos\theta_\mathrm{i}, \\ x_\mathrm{r} &= (x+s)\cos\theta_\mathrm{i} + (z-h)\sin\theta_\mathrm{i}, \\ z_\mathrm{r} &= (x+s)\sin\theta_\mathrm{i} - (z-h)\cos\theta_\mathrm{i}, \\ x_\mathrm{t} &= (x+s-l)\cos\theta_\mathrm{t} - (z+h')\sin\theta_\mathrm{t}, \\ z_\mathrm{t} &= (x+s-l)\sin\theta_\mathrm{t} + (z+h')\cos\theta_\mathrm{t}, \end{aligned} \tag{1}$$

where

$$\begin{aligned} &h' = h(k_3/k_1)(\cos^3\theta_\mathrm{t}/\cos^3\theta_\mathrm{i}), \\ &l = l' + l_0, \quad x_1 = x_0\cdot(\cos\theta_\mathrm{t}/\cos\theta_\mathrm{i}), \\ &l' = h\tan\theta_\mathrm{i} - h'\tan\theta_\mathrm{t}, \quad l_0 = d(\tan\theta_2 - \tan\theta_\mathrm{t}). \end{aligned} \tag{2}$$

Assuming a linearly polarized Airy beam is incident on a dielectric slab, whose waist is located at the inclined plane $z_\mathrm{i} = 0$. Along the $z_\mathrm{i} = 0$ plane, the electric field distribution of the Airy beam can be written as

$$E_\mathrm{w}(x_\mathrm{i}, 0) = \mathrm{Ai}\left(\frac{x_\mathrm{i}}{x_0}\right)\exp\left(a\frac{x_\mathrm{i}}{x_0}\right), \tag{3}$$

where x_0 denotes the beam width of the Airy beam, and a is the exponential decay factor varying from 0 to 1 to ensure the finite power of the Airy beam. A time dependence of $\exp(-\mathrm{i}\omega t)$ is omitted.

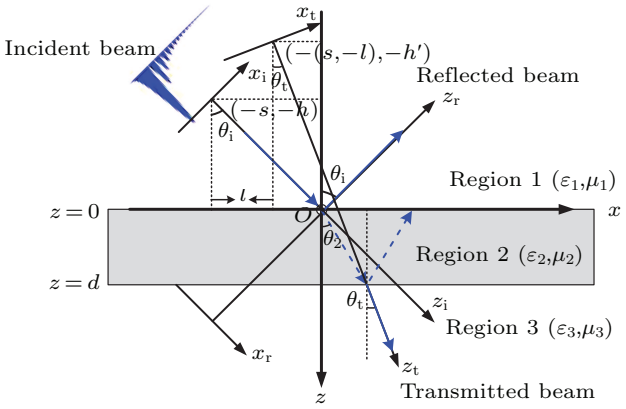


Fig. 1. Coordinate system for the reflection and transmission of a finite-power Airy beam impinging on a dielectric slab.

Rather than work with a field distribution along a plane $(z_\mathrm{i} = 0)$ that is not parallel to the dielectric interface $(z=0)$, it is more convenient to use the field distribution in the rotated aperture plane $(z=-h)$. The electric field distribution of the Airy beam in the aperture plane $z=-h$ is well approximated by

$$\begin{aligned} E_\mathrm{ap}(x,-h) &= [E_\mathrm{w}(x_\mathrm{i},0)\exp(\mathrm{i}k_1 z_\mathrm{i})]_{z=-h} \\ &= \mathrm{Ai}\left(\frac{(x+s)\cos\theta_\mathrm{i}}{x_0}\right)\exp\left(a\frac{(x+s)\cos\theta_\mathrm{i}}{x_0}\right) \\ &\quad\times\exp[\mathrm{i}k_1\sin\theta_\mathrm{i}(x+s)]. \end{aligned} \tag{4}$$

By using the Fourier transform, the spectral amplitude of the incident electric field at $z=-h$ can be expressed as

$$\begin{aligned} \Phi(k_x) &= \int_{-\infty}^{\infty} E_\mathrm{ap}(x,-h)\times\exp(-\mathrm{i}k_x x)\,\mathrm{d}x \\ &= \frac{x_0}{\cos\theta_\mathrm{i}}\exp\left[(a - \mathrm{i}\frac{(k_x - k_1\sin\theta_\mathrm{i})}{\cos\theta_\mathrm{i}}x_0)^3/3\right]\exp(\mathrm{i}k_x s). \end{aligned} \tag{5}$$

Based on the plane-wave angular spectrum expansion, the electric field components in each region can be derived by utilizing the integral inverse Fourier transformation. In the range of $-h < z < 0$, the incident electric field in the global coordinate can be derived as

$$E_{\mathrm{inc},j}(x,z) = \left(\frac{1}{2\pi}\right)\int_{-\infty}^{\infty} \Phi(k_x)\exp[\mathrm{i}(k_x x + k_{1z}h + k_{1z}z)]\,\mathrm{d}k_x. \quad (6)$$

Meanwhile, the reflected electric field above the first interface $z = 0$ is

$$\begin{aligned} &E_{\mathrm{ref},j}(x,z) \\ &= \left(\frac{1}{2\pi}\right)\int_{-\infty}^{\infty} r_j(k_x)\Phi(k_x)\exp[\mathrm{i}(k_x x + k_{1z}h - k_{1z}z)]\,\mathrm{d}k_x, \end{aligned} \quad (7)$$

where $r_j(k_x)$ is the generalized reflection coefficient.

In the global coordinate, the electric field distribution in the dielectric slab $E_{\mathrm{slab},j}(x,z)$ can be derived as[51]

$$\begin{aligned} E_{\mathrm{slab},j}(x,z) &= E_{\mathrm{d},j}(x,z) + E_{\mathrm{u},j}(x,z), \\ E_{\mathrm{d},j}(x,z) &= \left(\frac{1}{2\pi}\right)\int_{-\infty}^{\infty} A_{\mathrm{d},j}(k_x)\Phi(k_x) \\ &\quad \times \exp[\mathrm{i}(k_x x + k_{1z}h + k_{2z}z)]\,\mathrm{d}k_x, \\ E_{\mathrm{u},j}(x,z) &= \left(\frac{1}{2\pi}\right)\int_{-\infty}^{\infty} A_{\mathrm{u},j}(k_x)\Phi(k_x) \\ &\quad \times \exp[\mathrm{i}(k_x x + k_{1z}h - k_{2z}z)]\,\mathrm{d}k_x, \end{aligned} \quad (8)$$

where $E_{\mathrm{d},j}(x,z)$ and $E_{\mathrm{u},j}(x,z)$ denote the electric field components of the downgoing wave and upgoing wave in region 2, respectively. $A_{\mathrm{d},j}(k_x)$ and $A_{\mathrm{u},j}(k_x)$ are the coefficients of downgoing wave and upgoing wave, respectively.

The transmitted electric field in the region 3 can be expressed as

$$\begin{aligned} E_{\mathrm{tra},j}(x,z) &= \left(\frac{1}{2\pi}\right)\int_{-\infty}^{\infty} t_j(k_x)\Phi(k_x) \\ &\quad \times \exp[\mathrm{i}(k_x x + k_{1z}h + k_{3z}z)]\,\mathrm{d}k_x, \end{aligned} \quad (9)$$

where $j =$ p or s, p and s denote TM wave and TE wave, respectively. $t_j(k_x)$ is the generalized transmission coefficient. k_x is the wavenumber in the x direction, and k_{1z}, k_{2z}, and k_{3z} separately are the wavenumbers in each region in the z direction, which are related by the plane-wave dispersion relation

$$k_x^2 + k_{\beta z}^2 = k_\beta^2. \quad (10)$$

According to the boundary condition of electromagnetic fields, the generalized reflection coefficient $r_j(k_x)$ and the generalized transmission coefficient $t_j(k_x)$ for the three-layer medium can be defined as[52]

$$\begin{aligned} r_j(k_x) &= \frac{R_{12}^j + R_{23}^j\,\mathrm{e}^{\mathrm{i}2k_{2z}d}}{1 + R_{12}^j R_{23}^j\,\mathrm{e}^{\mathrm{i}2k_{2z}d}}, \\ t_j(k_x) &= \frac{T_{12}^j T_{23}^j\,\mathrm{e}^{\mathrm{i}(k_{2z}-k_{3z})d}}{1 + R_{12}^j R_{23}^j\,\mathrm{e}^{\mathrm{i}2k_{2z}d}}. \end{aligned} \quad (11)$$

Similarly, by matching the boundary conditions for the tangential electric and magnetic fields, the coefficients of downgoing wave $A_{\mathrm{d},j}(k_x)$ and upgoing wave $A_{\mathrm{u},j}(k_x)$ can be expressed as

$$\begin{aligned} A_{\mathrm{d},j}(k_x) &= \frac{T_{12}^j}{1 + R_{12}^j R_{23}^j\,\mathrm{e}^{\mathrm{i}2k_{2z}d}}, \\ A_{\mathrm{u},j}(k_x) &= \frac{T_{12}^j R_{23}^j\,\mathrm{e}^{\mathrm{i}2k_{2z}d}}{1 + R_{12}^j R_{23}^j\,\mathrm{e}^{\mathrm{i}2k_{2z}d}}. \end{aligned} \quad (12)$$

The R_{12}^j, R_{23}^j and T_{12}^j, T_{23}^j separately are the Fresnel reflection and transmission coefficients, which are given by

$$\begin{aligned} R_{\beta(\beta+1)}^j &= \frac{k_{\beta z} - m k_{(\beta+1)z}}{k_{\beta z} + m k_{(\beta+1)z}}, \quad m = \begin{cases} n_{\beta(\beta+1)}, & j = \mathrm{p}, \quad \text{parallel polarization.} \\ 1, & j = \mathrm{s}, \quad \text{vertical polarization,} \end{cases} \\ T_{\beta(\beta+1)}^j &= \frac{2k_{\beta z}}{k_{\beta z} + m k_{(\beta+1)z}}, \quad m = \begin{cases} n_{\beta(\beta+1)}, & j = \mathrm{p}, \quad \text{parallel polarization,} \\ 1, & j = \mathrm{s}, \quad \text{vertical polarization,} \end{cases} \end{aligned} \quad (13)$$

where $n_{\beta(\beta+1)} = (n_\beta / n_{\beta+1})^2$.

The integrals (6)–(9) need to be calculated over the entire real k_x axis. Whereas for the paraxial region, most of the contributions to results for values of k_x close to $k_{x0} = k_1 \sin\theta_{\mathrm{i}}$, and the contributions for $k_x \gg k_{x0}$ can be neglected. Employing the Fresnel approximation, the coefficients k_{1z}, k_{2z}, k_{3z} and $R_{\beta(\beta+1)}^j$, $T_{\beta(\beta+1)}^j$, $A_{\mathrm{d},j}(k_x)$, $A_{\mathrm{u},j}(k_x)$ are expanded as a Taylor series in k_x around the center angular component k_{x0}. Retaining up to quadratic terms, $k_{\beta z}$ can be expressed as

$$\begin{aligned} k_{\beta z} \approx\ & k_{\beta z}\Big|_{k_x = k_{x0}} + (k_x - k_{x0})k'_{\beta z}\Big|_{k_x = k_{x0}} \\ & + \frac{(k_x - k_{x0})^2}{2!}k''_{\beta z}\Big|_{k_x = k_{x0}}. \end{aligned} \quad (14)$$

We wish to evaluate the incident electric field by using the Fresnel approximation in Eq. (14), and it is more convenient

to define a new variable

$$\sigma = -\frac{k_x - k_1 \sin\theta_\mathrm{i}}{k_1 \cos\theta_\mathrm{i}}, \tag{15}$$

from which

$$k_x = k_1 \sin\theta_\mathrm{i} - \sigma k_1 \cos\theta_\mathrm{i}. \tag{16}$$

Substituting Eq. (15) into Eq. (14), we get

$$k_{1z} = \sqrt{k_1^2 - k_x^2} \approx k_1 \cos\theta_\mathrm{i} + \sigma k_1 \sin\theta_\mathrm{i} - \sigma^2 \frac{k_1}{2\cos\theta_\mathrm{i}}. \tag{17}$$

Substituting Eqs. (5) and (15)–(17) into Eq. (6), we get the expression for the incident electric field

$$\begin{aligned} E_{\mathrm{inc},j}(x_\mathrm{i}, z_\mathrm{i}) &= \frac{k_1 x_0}{2\pi} \exp(\mathrm{i}k_1 z_\mathrm{i}) \int_{-\infty}^{\infty} \exp\left[\frac{(a + \mathrm{i}k_1 x_0 \sigma)^3}{3}\right. \\ &\quad \left. - \frac{\mathrm{i}k_1(z+h)}{2\cos\theta_\mathrm{i}}\sigma^2 - \mathrm{i}k_1 x_\mathrm{i}\sigma\right] \mathrm{d}\sigma \\ &= \exp(\mathrm{i}k_1 z_\mathrm{i}) \mathrm{Ai}(M_1) \exp(\mathrm{i}N_1), \end{aligned} \tag{18}$$

where

$$\begin{aligned} A_1 &= \frac{1}{2k_1 x_0^2}(z_\mathrm{i} - x_\mathrm{i}\tan\theta_\mathrm{i}), \\ M_1 &= \frac{x_\mathrm{i}}{x_0} + 2\mathrm{i}A_1 a - A_1^2, \\ N_1 &= -\frac{2}{3}A_1^3 + 2\mathrm{i}A_1^2 a + \frac{x_\mathrm{i}}{x_0}A_1 + A_1 a^2 - \mathrm{i}a\frac{x_\mathrm{i}}{x_0}. \end{aligned} \tag{19}$$

For the reflected electric field, it is more complicated compared with the incident electric field due to the generalized reflection coefficient $r_j(k_x)$. $r_j(k_x)$ is expanded in a Taylor series as

$$\begin{aligned} r_j(k_x) &= r_j(k_x)\Big|_{k_x = k_{x0}} + (k_x - k_{x0}) r_j(k_x)'\Big|_{k_x = k_{x0}} \\ &\quad + \frac{(k_x - k_{x0})^2}{2!} r_j(k_x)''\Big|_{k_x = k_{x0}} + \cdots \end{aligned} \tag{20}$$

Substituting Eq. (15) into Eq. (20), we get

$$\begin{aligned} r_j(k_x) &= \sum_{n=0} \sigma^n B_n^j(\theta_\mathrm{i}), \\ B_n^j(\theta_\mathrm{i}) &= (-1)^n \frac{1}{n!}(k_1 \cos\theta_\mathrm{i})^n \frac{\partial^n}{\partial k_x^n} r_j(k_x)\big|_{k_x = k_{x0}}. \end{aligned} \tag{21}$$

Substituting Eqs. (5), (16), (17) and (21) into Eq. (7), the reflected electric field can be calculated by using the differential properties of Fourier Transform. We obtain the following result:

$$E_{\mathrm{ref},j}(x_\mathrm{r}, z_\mathrm{r}) = \sum_{n=0} E_{\mathrm{r}n,j}(x_\mathrm{r}, z_\mathrm{r}) = \frac{k_1 x_0}{2\pi} \exp(\mathrm{i}k_1 z_\mathrm{r}) \int_{-\infty}^{\infty} \left[\sum_{n=0} \sigma^n B_n^j(\theta_\mathrm{i})\right] \exp\left[\frac{(a + \mathrm{i}k_1 x_0 \sigma)^3}{3} + \frac{\mathrm{i}k_1(z-h)}{2\cos\theta_\mathrm{i}}\sigma^2 - \mathrm{i}k_1 x_\mathrm{r}\sigma\right] \mathrm{d}\sigma, \tag{22}$$

where

$$E_{\mathrm{r}n,j}(x_\mathrm{r}, z_\mathrm{r}) = \frac{\exp(\mathrm{i}k_1 z_\mathrm{r})}{(k_1 x_0)^n} B_n^j(\theta_\mathrm{i}) \sum_{m=0}^{n} \mathrm{C}_n^m (\mathrm{i}a)^{n-m} (-\mathrm{i})^m \frac{\mathrm{d}^m \{\exp[\mathrm{i}(\frac{2}{3}A_2^3 + A_2 w_2 - A_2 a^2 - \mathrm{i}a\frac{x_\mathrm{r}}{x_0})]\mathrm{Ai}(-w_2 - A_2^2)\}}{\mathrm{d}w_2^m}, \tag{23}$$

and $w_2 = -(x_\mathrm{r}/x_0 - 2\mathrm{i}A_2 a)$.

Due to the nonlinear properties of the generalized reflection coefficient $r_j(k_x)$, the structure of the reflected field is different from the incident field. In addition to the fundamental reflected beam mode $E_{\mathrm{r}0,j}$, higher order reflected beam modes $E_{\mathrm{r}n,j}$ are generated.

$$\begin{aligned} E_{\mathrm{r}0,j}(x_\mathrm{r}, z_\mathrm{r}) &= \exp(\mathrm{i}k_1 z_\mathrm{r}) \exp(\mathrm{i}N_2) B_0^j(\theta_\mathrm{i}) \mathrm{Ai}(M_2), \\ E_{\mathrm{r}1,j}(x_\mathrm{r}, z_\mathrm{r}) &= \frac{\exp(\mathrm{i}k_1 z_\mathrm{r})}{k_1 x_0} \exp(\mathrm{i}N_2) B_1^j(\theta_\mathrm{i}) \\ &\quad \times [(\mathrm{i}a + A_2)\mathrm{Ai}(M_2) + \mathrm{i}\mathrm{Ai}'(M_2)], \end{aligned} \tag{24}$$

where $E_{\mathrm{r}0,j}$ denotes the geometrically reflected beam field, and $E_{\mathrm{r}1,j}$ denotes the first order reflected beam mode field. The relevant parameters are expressed as follows:

$$\begin{aligned} A_2 &= -\frac{1}{2k_1 x_0^2}(z_\mathrm{r} - x_\mathrm{r}\tan\theta_\mathrm{i}), \\ M_2 &= \frac{x_\mathrm{r}}{x_0} - 2\mathrm{i}A_2 a - A_2^2, \\ N_2 &= \frac{2}{3}A_2^3 + 2\mathrm{i}A_2^2 a - \frac{x_\mathrm{r}}{x_0}A_2 - A_2 a^2 - \mathrm{i}a\frac{x_\mathrm{r}}{x_0}. \end{aligned} \tag{25}$$

For the transmitted beam, most of the contributions to Eq. (9) result from the region around the transmitted beam axis. By Snell's law, we obtain $k_{x0} = k_1 \sin\theta_\mathrm{i} = k_3 \sin\theta_\mathrm{t}$. To calculate the transmitted electric field easily, a new variable of integration is introduced

$$\tau = -\frac{k_x - k_3 \sin\theta_\mathrm{t}}{k_3 \cos\theta_\mathrm{t}}, \tag{26}$$

from which

$$k_x = k_3 \sin\theta_\mathrm{t} - \tau k_3 \cos\theta_\mathrm{t}. \tag{27}$$

Substituting Eq. (26) into Eq. (14), we get

$$\begin{aligned} k_{1z} &= \sqrt{k_1^2 - k_x^2} \approx k_1 \cos\theta_\mathrm{i} + \tau k_3 \cos\theta_\mathrm{t} \tan\theta_\mathrm{i} - \tau^2 \frac{k_3^2 \cos^2\theta_\mathrm{t}}{2k_1 \cos^3\theta_\mathrm{i}}, \\ k_{3z} &= \sqrt{k_3^2 - k_x^2} \approx k_3 \cos\theta_\mathrm{t} + \tau k_3 \sin\theta_\mathrm{t} - \tau^2 \frac{k_3}{2\cos\theta_\mathrm{t}}. \end{aligned} \tag{28}$$

Similar to the $r_j(k_x)$, the generalized transmission coefficient $t_j(k_x)$ can be expressed in a Taylor series as

$$t_j(k_x) = \sum_{n=0} \tau^n D_n^j(\theta_t),$$

$$D_n^j(\theta_t) = (-1)^n \frac{1}{n!}(k_3\cos\theta_t)^n \frac{\partial^n}{\partial k_x^n} t_j(k_x)\big|_{k_x=k_{x0}}. \quad (29)$$

Similar to the reflected electric field, by substituting Eqs. (5) and (27)–(29) into Eq. (9), the expression for the transmitted electric field can be given as

$$\begin{aligned} E_{\mathrm{tra},j}(x_t,z_t) &= \frac{k_3x_1}{2\pi}\exp(\mathrm{i}k_3(z_t+l_0\sin\theta_t))\exp\left(\frac{\mathrm{i}k_1h}{\cos\theta_i}-\frac{\mathrm{i}k_3h'}{\cos\theta_t}\right) \\ &\times\int_{-\infty}^{\infty}\left[\sum_{n=0}\tau^n D_n^j(\theta_t)\right]\cdot\exp\left[\frac{(a+\mathrm{i}k_3x_1\tau)^3}{3}-\frac{\mathrm{i}k_3(z+h')}{2\cos\theta_t}\tau^2-\mathrm{i}k_3(x_t+l_0\cos\theta_t)\tau\right]\mathrm{d}\tau = \sum_{n=0}E_{tn,j}(x_t,z_t), \end{aligned} \quad (30)$$

where

$$\begin{aligned} E_{tn,j}(x_t,z_t) &= \exp\left(\frac{\mathrm{i}k_1h}{\cos\theta_i}-\frac{\mathrm{i}k_3h'}{\cos\theta_t}\right)\frac{\exp(\mathrm{i}k_3(z_t+l_0\sin\theta_t))}{(k_3x_1)^n}D_n^j(\theta_t) \\ &\times\sum_{m=0}^{n}\mathrm{C}_n^m(\mathrm{i}a)^{n-m}(-\mathrm{i})^m\frac{\mathrm{d}^m\{\exp[\mathrm{i}(-\frac{2}{3}A_3^3-A_3w_3+A_3a^2-\mathrm{i}a\frac{(x_t+l_0\cos\theta_t)}{x_1})]\mathrm{Ai}(-w_3-A_3^2)\}}{\mathrm{d}w_3^m} \end{aligned} \quad (31)$$

and $w_3 = -(2\mathrm{i}A_3a+(x_t+l_0\cos\theta_t)/x_1)$.

The geometrically transmitted beam field $E_{t0,j}$ and first order transmitted beam mode field $E_{t1,j}$ can be expressed as

$$\begin{aligned} E_{t0,j}(x_t,z_t) &= \exp(\frac{\mathrm{i}k_1h}{\cos\theta_i}-\frac{\mathrm{i}k_3h'}{\cos\theta_t})\exp(\mathrm{i}k_3(z_t+l_0\sin\theta_t)) \\ &\times\exp(\mathrm{i}N_3)D_0^j(\theta_t)\mathrm{Ai}(M_3), \\ E_{t1,j}(x_t,z_t) &= \exp(\frac{\mathrm{i}k_1h}{\cos\theta_i}-\frac{\mathrm{i}k_3h'}{\cos\theta_t})\frac{\exp(\mathrm{i}k_3(z_t+l_0\sin\theta_t))}{k_3x_1} \\ &\times\exp(\mathrm{i}N_3)D_1^j(\theta_t) \\ &\times[(\mathrm{i}a-A_3)\mathrm{Ai}(M_3)+\mathrm{i}\mathrm{Ai}'(M_3)], \end{aligned} \quad (32)$$

where

$$A_3 = \frac{1}{2k_3x_1^2}(z_t-(x_t+l_0\cos\theta_t)\tan\theta_t),$$

$$\begin{aligned} M_3 &= \frac{(x_t+l_0\cos\theta_t)}{x_1}+2\mathrm{i}A_3a-A_3^2, \\ N_3 &= -\frac{2}{3}A_3^3+2\mathrm{i}A_3^2a+\frac{(x_t+l_0\cos\theta_t)}{x_1}A_3 \\ &\quad +A_3a^2-\mathrm{i}a\frac{(x_t+l_0\cos\theta_t)}{x_1}. \end{aligned} \quad (33)$$

In the same way, the electric field in the dielectric slab can be derived as

$$\begin{aligned} E_{\mathrm{slab},j}(x,z) &= E_{\mathrm{d},j}(x,z)+E_{\mathrm{u},j}(x,z), \\ E_{\mathrm{d},j}(x,z) &= \sum_{n=0}E_{\mathrm{d}n,j}(x,z), \\ E_{\mathrm{u},j}(x,z) &= \sum_{n=0}E_{\mathrm{u}n,j}(x,z), \end{aligned} \quad (34)$$

$$\begin{aligned} E_{\mathrm{d}n,j}(x,z) &= \exp\left(\frac{\mathrm{i}k_1h}{\cos\theta_i}-\frac{\mathrm{i}k_2h_2}{\cos\theta_2}\right)\exp(\mathrm{i}k_2z_2)(\frac{1}{k_2x_1'})^nC_n^j(\theta_2) \\ &\times\sum_{m=0}^{n}\mathrm{C}_n^m(\mathrm{i}a)^{n-m}(-\mathrm{i})^m\frac{\mathrm{d}^m\{\exp[\mathrm{i}(-\frac{2}{3}A_4^3-A_4w_4+A_4a^2-\mathrm{i}a\frac{x_2}{x_1'})]\mathrm{Ai}(-w_4-A_4^2)\}}{\mathrm{d}w_4^m}, \\ E_{\mathrm{u}n,j}(x,z) &= \exp\left(\frac{\mathrm{i}k_1h}{\cos\theta_i}-\frac{\mathrm{i}k_2h_2}{\cos\theta_2}-2\mathrm{i}k_2\cos\theta_2z\right)\exp(\mathrm{i}k_2z_2)\left(\frac{1}{k_2x_1'}\right)^nQ_n^j(\theta_2) \\ &\times\sum_{m=0}^{n}\mathrm{C}_n^m(\mathrm{i}a)^{n-m}(-\mathrm{i})^m\frac{\mathrm{d}^m\{\exp[\mathrm{i}(-\frac{2}{3}A_4'^3-A_4'w_4'+A_4'a^2-\mathrm{i}a\frac{x_2-2\sin\theta_2z}{x_1'})]\mathrm{Ai}(-w_4'-A_4'^2)\}}{\mathrm{d}w_4'^m}, \end{aligned} \quad (35)$$

$$w_4 = -\left(2\mathrm{i}A_4a+\frac{x_2}{x_1'}\right), \quad w_4' = -\left(\frac{x_2-2\sin\theta_2z}{x_1'}+2\mathrm{i}A_4'a\right).$$

The zero and first order beam mode fields of the downgoing wave and upgoing wave can be written as

$$E_{\mathrm{d}0,j}(x,z) = \exp\left(\frac{\mathrm{i}k_1h}{\cos\theta_i}-\frac{\mathrm{i}k_2h_2}{\cos\theta_2}\right)\exp(\mathrm{i}k_2z_2)\exp(\mathrm{i}N_4)C_0^j(\theta_2)\mathrm{Ai}(M_4),$$

$$
\begin{aligned}
E_{\mathrm{d1},j}(x,z) &= \exp\left(\frac{\mathrm{i}k_1h}{\cos\theta_\mathrm{i}}-\frac{\mathrm{i}k_2h_2}{\cos\theta_2}\right)\frac{\exp(\mathrm{i}k_2z_2)}{k_2x_1'}\exp(\mathrm{i}N_4)C_1^j(\theta_2)[(\mathrm{i}a-A_4)\mathrm{Ai}(M_4)+\mathrm{i}\mathrm{Ai}'(M_4)],\\
E_{\mathrm{u}0,j}(x,z) &= \exp\left(\frac{\mathrm{i}k_1h}{\cos\theta_\mathrm{i}}-\frac{\mathrm{i}k_2h_2}{\cos\theta_2}-2\mathrm{i}k_2\cos\theta_2z\right)\exp(\mathrm{i}k_2z_2)\exp(\mathrm{i}N_4')Q_0^j(\theta_2)\mathrm{Ai}(M_4'),\\
E_{\mathrm{u}1,j}(x,z) &= \exp\left(\frac{\mathrm{i}k_1h}{\cos\theta_\mathrm{i}}-\frac{\mathrm{i}k_2h_2}{\cos\theta_2}-2\mathrm{i}k_2\cos\theta_2z\right)\frac{\exp(\mathrm{i}k_2z_2)}{k_2x_1'}\exp(\mathrm{i}N_4')Q_1^j(\theta_2)[(\mathrm{i}a-A_4')\mathrm{Ai}(M_4')+\mathrm{i}\mathrm{Ai}'(M_4')],
\end{aligned}
\tag{36}
$$

where

$$
\begin{aligned}
x_2 &= (x+s-l_2)\cos\theta_2-(z+h_2)\sin\theta_2,\\
z_2 &= (x+s-l_2)\sin\theta_2+(z+h_2)\cos\theta_2,\\
x_1' &= x_0\cdot(\cos\theta_2/\cos\theta_\mathrm{i}),\\
h_2 &= h(k_2/k_1)(\cos^3\theta_2/\cos^3\theta_\mathrm{i}),\\
l_2 &= h\tan\theta_\mathrm{i}-h_2\tan\theta_2,\\
A_4 &= \frac{1}{2k_2x_1'^2}\cdot\frac{z+h_2}{\cos\theta_2},\\
A_4' &= \frac{1}{2k_2x_1'^2}\cdot\frac{-z+h_2}{\cos\theta_2},\\
M_4 &= \frac{x_2}{x_1'}+2\mathrm{i}A_4a-A_4^2,\\
M_{4'} &= \frac{x_2-2\sin\theta_2z}{x_1'}+2\mathrm{i}A_4'a-A_4'^2,\\
N_4 &= -\frac{2}{3}A_4^3+2\mathrm{i}A_4^2a+\frac{x_2}{x_1'}A_4+A_4a^2-\mathrm{i}a\frac{x_2}{x_1'},\\
N_4' &= -\frac{2}{3}A_4'^3+2\mathrm{i}A_4'^2a+\frac{x_2-2\sin\theta_2z}{x_1'}A_4'\\
&\quad +A_4'a^2-\mathrm{i}a\frac{x_2-2\sin\theta_2z}{x_1'}.
\end{aligned}
\tag{37}
$$

The Taylor expansion coefficients of the downgoing wave and upgoing wave can be denoted as

$$
\begin{aligned}
C_n^j(\theta_2) &= (-1)^n\frac{1}{n!}(k_2\cos\theta_2)^n\frac{\partial^n}{\partial k_x^n}A_{\mathrm{d},j}(k_x)\big|_{k_x=k_{x0}},\\
Q_n^j(\theta_2) &= (-1)^n\frac{1}{n!}(k_2\cos\theta_2)^n\frac{\partial^n}{\partial k_x^n}A_{\mathrm{u},j}(k_x)\big|_{k_x=k_{x0}}.
\end{aligned}
\tag{39}
$$

3. Numerical results and discussion

In this section, the characteristics of an Airy beam incident on a dielectric slab are simulated and discussed. In the following discussion we only consider a p-polarized Airy beam, with $x_0=20$ μm, and $a=0.08$. The wavelength of incident beam is $\lambda_0=500$ nm, and the thickness of the dielectric slab is $d=50\lambda_0$. The refractive indices are set to $n_1=1.5$ and $n_3=1$, respectively. The diffraction length of the beam in region 1 is $L_{\mathrm{d}1}=k_1x_0^2$. Here we set $h=L_{\mathrm{d}1}\cos\theta_\mathrm{i}$, which allows the beam to propagate for one diffraction length before it hits the first interface $z=0$. We retain the first two terms of the electric field expression, and the actual beam field is the sum of the geometrically beam field and first order beam mode field. The incident, reflected and transmitted beam axes predicted by Snell's law separately are $\chi_\mathrm{i}=x-z\tan\theta_\mathrm{i}$, $\chi_\mathrm{r}=x+z\tan\theta_\mathrm{i}$ and $\chi_\mathrm{t}=(x-l_0)-z\tan\theta_\mathrm{t}$,[43] respectively. In what follows, we present the intensity distributions of the incident, reflected and transmitted beams in coordinates (χ_i,z), (χ_r,z), and (χ_t,z), respectively.

3.1. Intensity distributions of the incident, reflected, internal and transmitted beams

According to Eq. (18), the intensity distributions of the incident beams with different incident angles are shown in Fig. 2. It is easy to find that the intensity distribution of the incident beam will not change with increase of the propagation distance due to the nondiffracting property of the Airy beam. Comparing Fig. 2(a) with Figs. 2(b) and 2(c), we can see that as the incident angles increase, the distribution area of the incident Airy beam becomes wider, but the magnitude of the incident beam will not change. Therefore, the change in incident angles will affect the width of the incident beam, but will not change the amplitude.

The intensity distributions of the reflected and transmitted beams through a dielectric slab with different refractive index n_2 are shown in Fig. 3.

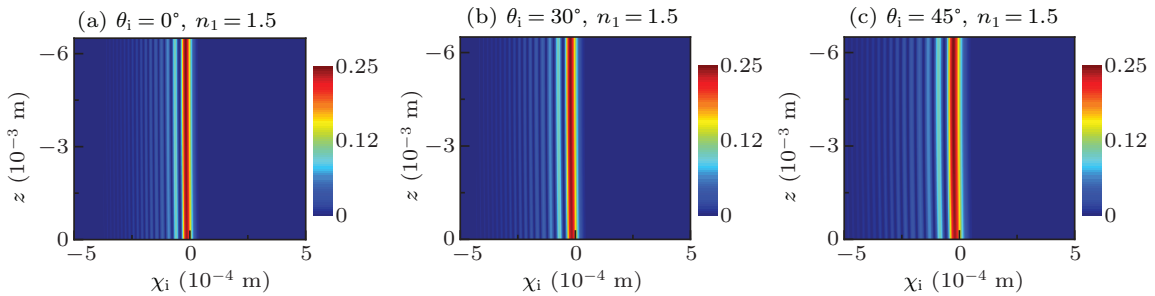


Fig. 2. Intensity distributions of the incident beams. The incident angles of the incident beams for (a), (b) and (c) are 0°, 30°, 45°, respectively.

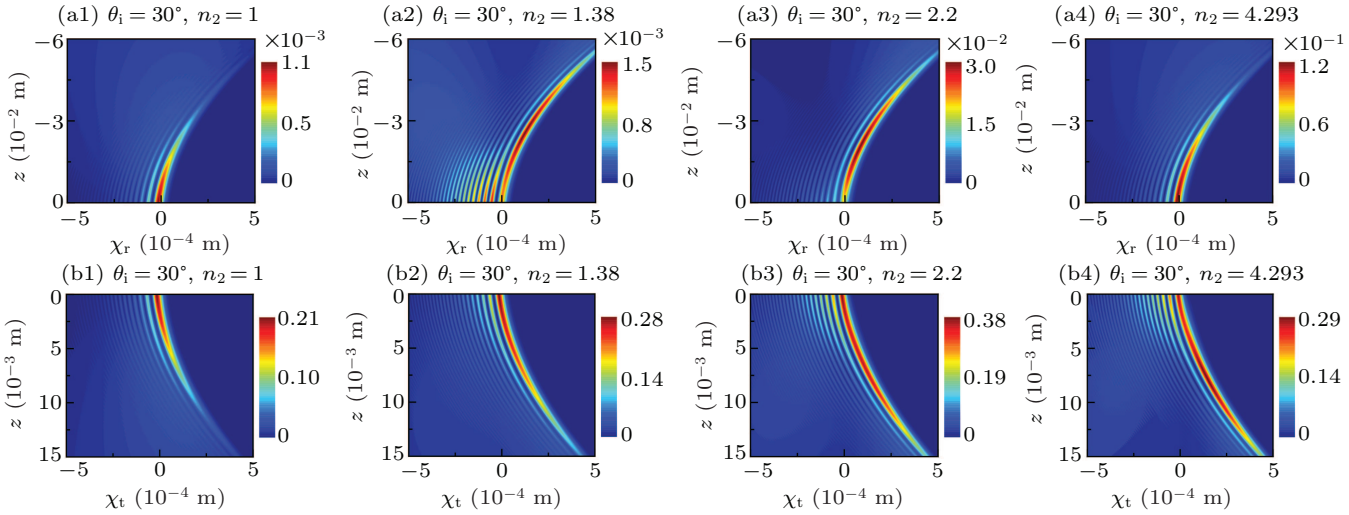


Fig. 3. Impinging at angle $\theta_i = 30°$, intensity distributions of the reflected and transmitted beams. The first row is the reflected beams, and the second row is the transmitted beams. The refractive index of the dielectric slab for (a1), (b1); (a2), (b2); (a3), (b3); and (a4), (b4) is $n_2 = 1$, (air), $n_2 = 1.38$ (MgF_2), $n_2 = 2.2$ ($LiNbO_3$) and $n_2 = 4.293$ (Si), respectively.

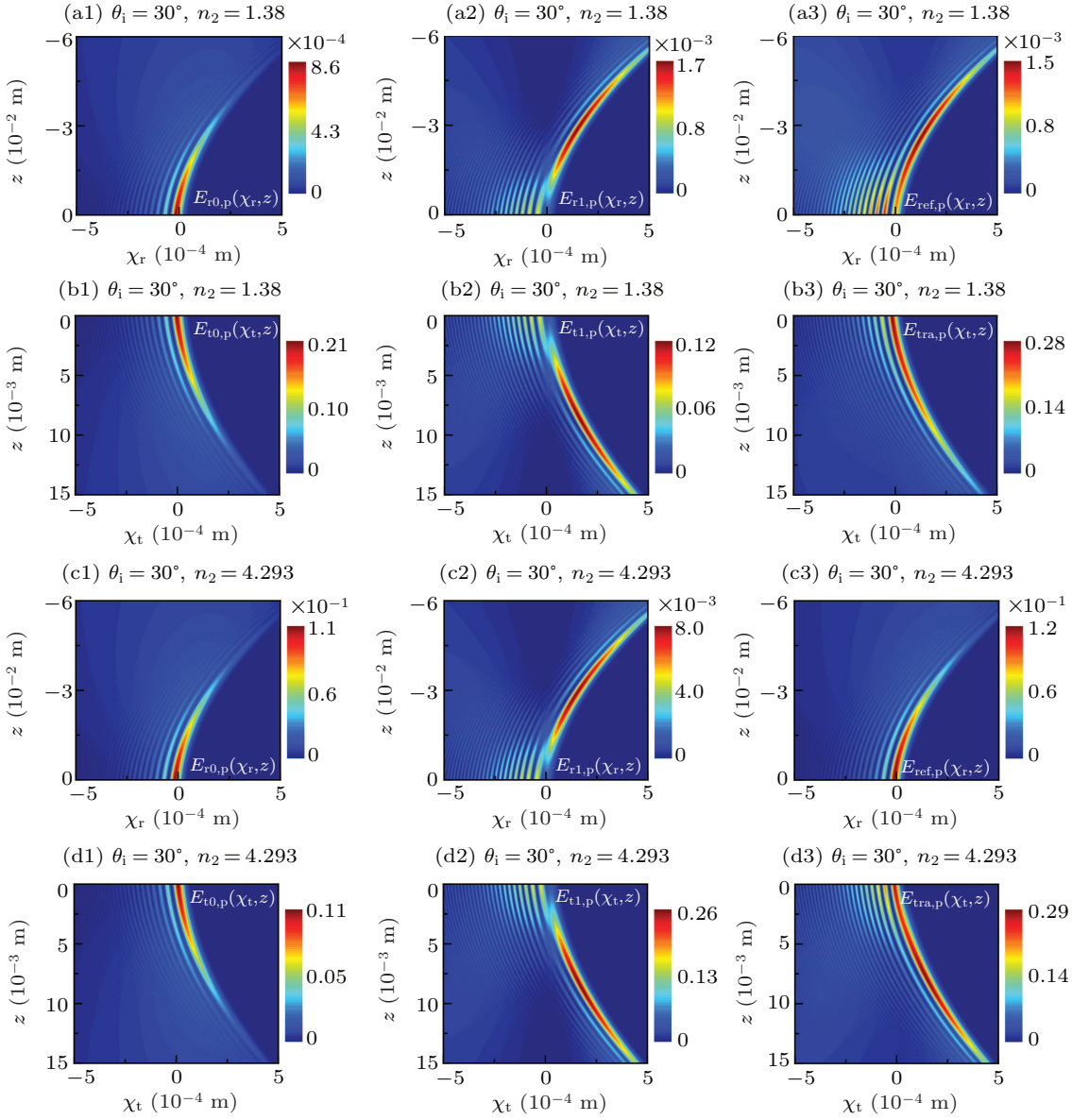


Fig. 4. Impinging at angle $\theta_i = 30°$, intensity distributions of (a1)–(d1) for the geometrically beam field, (a2)–(d2) for first order beam mode field and (a3)–(d3) for actual beam field with $n_2 = 1.38$ and $n_2 = 4.293$, respectively. The first and third rows are the reflected beams, and the second and fourth rows are the transmitted beams.

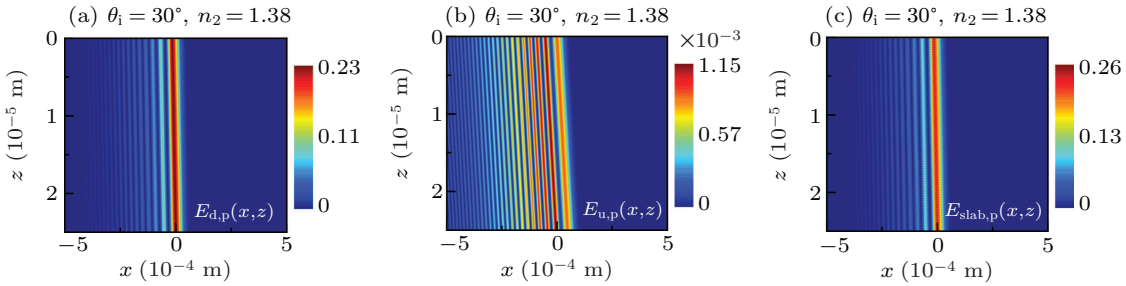


Fig. 5. Impinging at angle $\theta_i = 30°$, intensity distributions of (a) the downgoing wave, (b) upgoing wave and (c) total beam in the dielectric slab with $n_2 = 1.38$.

When the refractive index of the dielectric slab $n_2 = 1$, it degrades to a half-space interface. Thus, by comparing Figs. 3(a1) and 3(b1) with the results shown in Ref. [43], the correctness of the method provided in this paper can be verified. In Fig. 3, It is obvious that both reflected and transmitted beams are Airy-like and exhibit accelerating dynamics along the transverse direction like the incident beam. From Figs. 3(a1)–3(a4), we can find that the main lobe's intensity of the reflected beam increases with the refractive index n_2 increasing. At $n_2 = 1.38$, the side lobe's intensity of the reflected beam is significantly enhanced. Furthermore, due to the small Fresnel reflection coefficient, the intensity of the transmitted beam is much greater than that of the reflected beam no matter how the refractive index changes in region 2. In Figs. 3(b1)–3(b4), for the transmitted beam, we can find that with the refractive index n_2 increasing, the diffraction speed of the main lobe becomes slower.

Based on the Eqs. (24) and (32), we study the intensity distributions of the geometrical-optics beam field, first order beam mode field and actual beam field of the Airy beams propagating through a dielectric slab with different refractive index n_2 in Fig. 4. From Figs. 4(a1)–4(d1) and 4(a2)–4(d2), we can see that the intensity distributions of the geometrical-optics reflected and transmitted beam field still maintain Airy-like shape, while the intensity distributions of the first order reflected and transmitted beam mode field are significantly distorted, whose initial amplitude profile is severely destructed. For the reflected beams, comparing Figs. 4(a1)–4(a3) with Figs. 4(c1)–4(c3), we can find that the intensity of the first order beam mode field is greater than the intensity of geometrical-optics beam field at $n_2 = 1.38$, and the intensity of actual beam field mainly depends on the intensity of first order beam field, while at $n_2 = 4.293$, the intensity of the first order beam mode field is smaller than the intensity of geometrical-optics beam field, the intensity of actual beam field mainly depends on the intensity of geometrical-optics beam field. The change of refractive index n_2 will affect the generalized reflection coefficient of the dielectric slab, and thus affect the intensity of each order beam mode field. Therefore, the refractive index n_2 will affect the contribution of each order beam mode field to the actual beam field. The similar conclusion also applies to the transmitted beam case.

With Eq. (34), in the global coordinate (x,z), the intensity distributions of the downgoing wave, upgoing wave and total beam in the dielectric slab at oblique incidence are presented in Fig. 5. The intensity distribution of the total beam in the dielectric slab is similar to the incident beam. Comparing Fig. 5(a) with Fig. 5(b), we can find that the downgoing wave intensity is much greater than the upgoing wave intensity. The intensity distributions of the total beam and downgoing wave in the dielectric slab are almost the same, which proves that the total beam intensity in the dielectric slab mainly depends on the downgoing wave in the case of incident angle $\theta_i = 30°$ and refractive index of the dielectric slab $n_2 = 1.38$.

3.2. Characteristics of the reflected beam at Brewster incidence and total reflection

It is also of interest to investigate the cases when Brewster incidence and total reflection take place on the first interface. To satisfy the condition $n_2 < n_1 \sin\theta_i < n_3$,[21] the refractive indices are chosen to be $n_1 = 1.5$, $n_2 = 1.38$ and $n_3 = 1.45$ (SiO_2). The intensity distribution of the reflected beam when the Airy beam is incident under Brewster angle $\theta_B = 42.61°$ in the first interface is shown in Fig. 6. From Fig. 6(a), we can find that the Airy shape of the reflected beam is distorted severely at polarizing incidence, and on the interface $z = 0$ the main lobe of the beam nearly disappears but the number of side lobes increases, which is due to the Fresnel reflection coefficient R_{12}^{p} has a zero at $\theta_B = 42.61°$. Figure 6(b) shows the amplitude profiles of the reflected beam at different propagation distances. The initial amplitude profile is severely disturbed, while the features of Airy profile gradually recover as the beam propagates to $z = -2$ cm, which verifies the self-healing property of the Airy beam.

The case when total reflection takes place on the first interface is presented in Fig. 7. The critical angle of total internal reflection is $\theta_c = 66.93°$. Figure 7(a) shows the intensity distribution of the reflected beam in the total internal reflection case, which is a clear Airy-like shape and accelerates toward Snell's reflection axis. The reflected beam will suffer the Goos–Hänchen shift in the total internal reflection as shown in

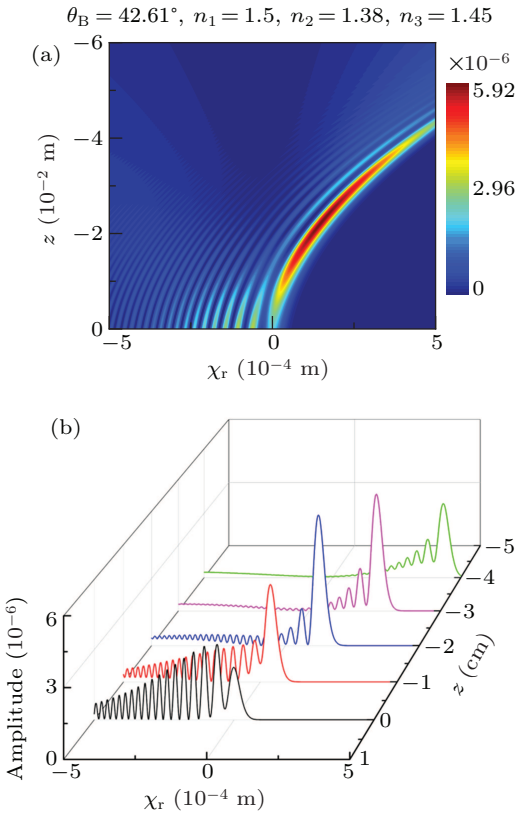


Fig. 6. Impinging at Brewster angle $\theta_B = 42.61°$, (a) intensity distribution of the reflected beam. (b) Amplitude profiles of the reflected beam versus position χ_r from Snell's reflection axis at different propagation distances.

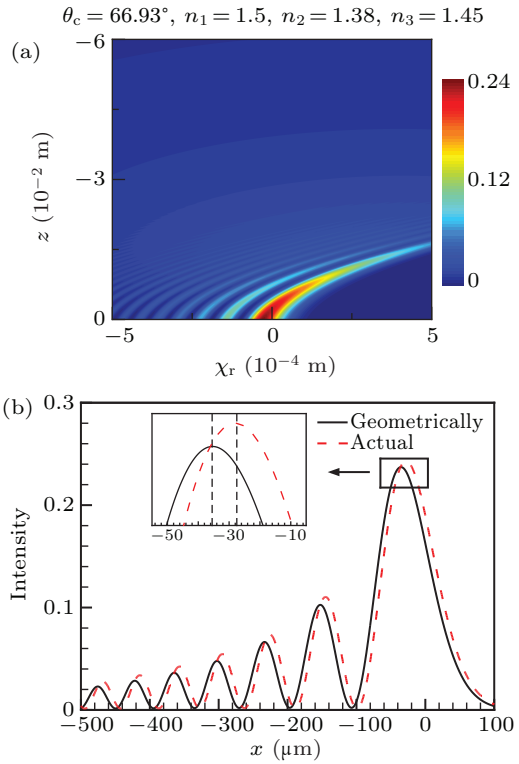


Fig. 7. Impinging at critical angle $\theta_c = 66.93°$. (a) Intensity distribution of the reflected beam. (b) The amplitude profiles of the geometrically reflected beam (solid) and actual reflected beam (dashed) on the interface $z = 0$, providing evidence to the Goos–Hänchen shift.

Fig. 7(b). We choose the peak of the reflected beam intensity as the reference point to investigate the lateral shift of the Airy beam,[53] and the shift is shown in the enlarged figure in Fig. 7(b). The Goos–Hänchen shift is calculated to be 8 μm or approximately 16 wavelengths.

3.3. Effects of optical thickness and refractive index of the dielectric slab

Next, we investigate the effects of the optical thickness of the dielectric slab on the intensity distributions of the reflected and transmitted beams. Here the optical thickness of the dielectric slab is $H = n_2 d$. Peak intensity is the maximum value of the beam intensity in the (x,z)-plane. Figure 8 shows the peak intensity of the reflected and transmitted beams varying with the optical thickness of the dielectric slab in different refractive index n_2 for normal incidence. The peak intensity of the reflected and transmitted beams varies periodically with the optical thickness of the dielectric slab, whose period is a half of the wavelength, so the dielectric slab whose optical thickness is $H = m\lambda_0/2$ (where $m = 1,2,3$) has no influence on the peak intensity of the reflected and transmitted beams. At $n_2 = 1$, the dielectric slab degrades to a half-space interface and the peak intensity will not be affect by the optical thickness of the dielectric slab. For the reflected beam, when $n_2 = 2.2$ and 4.293, the peak intensity is a maximum with the dielectric slab whose optical thickness is $H = m\lambda_0/4$ (where $m = 1,3,5$). On the contrary, when $n_2 = 1.38$ and 1.45, the peak intensity reaches the minimum with the dielectric slab whose optical thickness is $H = m\lambda_0/4$ (where $m = 1,3,5$), and the peak intensity

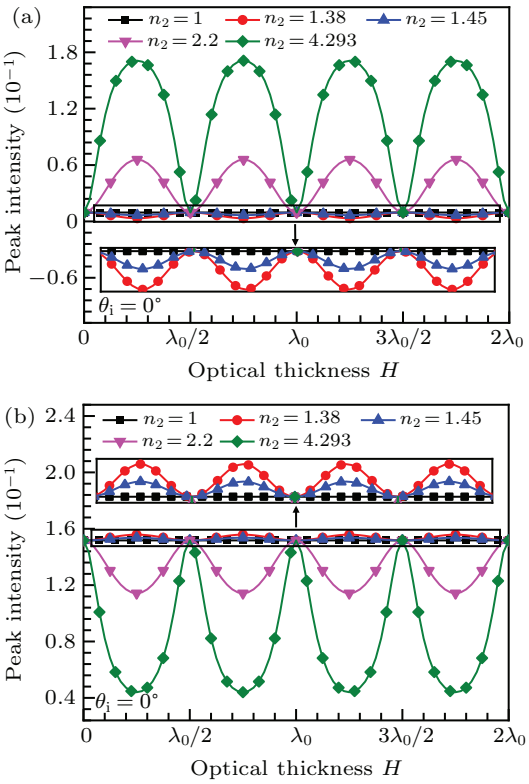


Fig. 8. At normal incidence, peak intensity distributions of (a) reflected beam and (b) transmitted beam as a function of the optical thickness of the dielectric slab for different refractive index n_2.

is minimum at $n_2 = 1.38$ because $n_2 = 1.38$ is closest to $n_2 = \sqrt{n_1 n_3} \approx 1.22$ at which the reflectivity is equal to zero for normal incidence.[21] For the transmitted beam, the variation of the peak intensity with the optical thickness of the dielectric slab is exactly opposite to the peak intensity of the reflected beam.

Figure 9 shows that the peak intensity of the reflected and transmitted beams varying with the optical thickness of the dielectric slab in different refractive index n_2 at incident angle $\theta_i = 30°$. Comparing Figs. 8(a) and 8(b) with Figs. 9(a) and 9(b), we can find that at oblique incidence the peak intensity of the reflected and transmitted beams also varies periodically with the optical thickness of the dielectric slab but the period has changed, which is $\lambda_0/2\cos\theta_2$, and the extreme values of the peak intensity of the reflected and transmitted beams also change. The variation trend of the peak intensity of the reflected and transmitted beams with the optical thickness of the dielectric slab at oblique incidence is the same as that at normal incidence at $n_2 = 1.38$, 1.45, 2.2, and 4.293. As to the effect of the refractive index n_2 of the dielectric slab on the peak intensity distributions of the reflected and transmitted beams, we proceed to discuss in the following part.

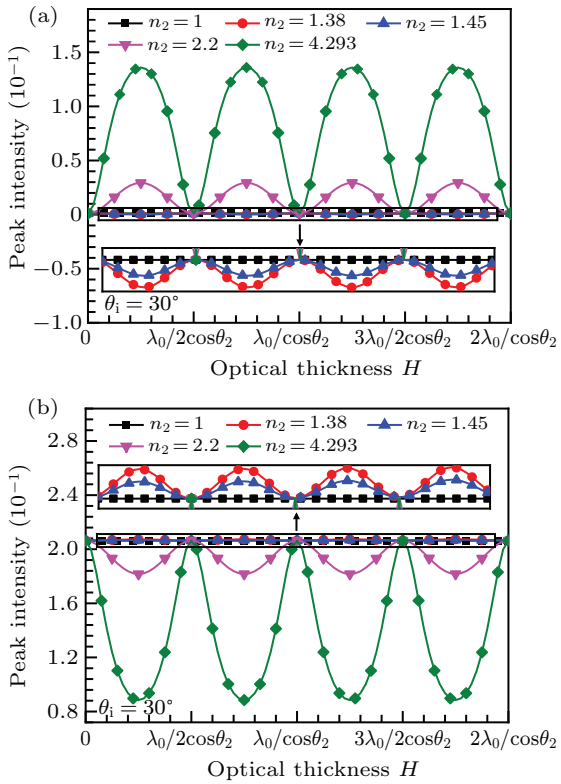


Fig. 9. Impinging at angle $\theta_i = 30°$, peak intensity distribution of (a) reflected beam and (b) transmitted beam as a function of the optical thickness of the dielectric slab for different refractive index n_2.

In order to further analyze the influence of the refractive index on the intensity distribution of the Airy beam through a dielectric slab, under special optical thickness and incident angle, the peak intensity distributions of reflected and transmitted beams varying with the refractive index n_2 of the dielectric slab are presented in Fig. 10. I_r and I_t denote the peak intensity of the reflected and transmitted beams, respectively. From Fig. 10(a), we can see that at normal incidence, the peak intensity of the reflected beam initially decreases and then increases with the refractive index n_2 increasing, while the change of the peak intensity of the transmitted beam is exactly opposite. At $n_2 = 1.22$, the peak intensity of the reflected beam reaches the minimum but the peak intensity of the transmitted beam reaches the maximum, which can be used as an antireflection film. In Fig. 10(b), at incident angle $\theta_i = 30°$, the peak intensity of the reflected beam first increases, then decreases and increases again, which is different from the case of normal incidence. Likewise, the change of the peak intensity of the transmitted beam is opposite to the peak intensity of the reflected beam. At $n_2 = 1.35$, the peak intensity of the reflected beam reaches the minimum and the peak intensity of the transmitted beam reaches the maximum. By choosing suitable material and thickness of the dielectric slab, many useful applications can be obtained in optical film.

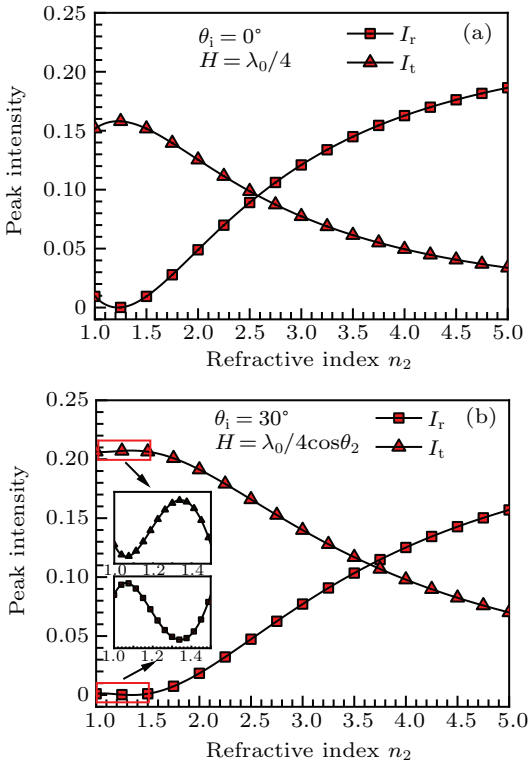


Fig. 10. At normal incidence ($\theta_i = 0°$) and oblique incidence ($\theta_i = 30°$), peak intensity distributions of the reflected and transmitted beams as a function of the refractive index n_2 of the dielectric slab. The optical thickness of the dielectric slab for (a) and (b) are $H = \lambda_0/4$ and $H = \lambda_0/4\cos\theta_2$, respectively.

Since there are no beam shifts for the reflected and transmitted beams at normal incidence, we analyze the effects of the optical thickness and refractive index of the dielectric slab on the beam shifts of the reflected and transmitted beams at incident angle $\theta_i = 30°$. As mentioned above, we choose the

peak of the geometrically reflected beam and actual reflected beam on the interface $z = 0$ as the reference point to investigate the lateral shift of the Airy beam.[53] Figure 11(a) shows that the variations of the beam shifts of the reflected and transmitted beams with the optical thickness of the dielectric slab in refractive index $n_2 = 1.45$ and incident angle $\theta_i = 30°$. We can notice that the beam shift of the reflected beam is on the rise overall, and there is an extreme value of the beam shift in every period $T = \lambda_0/2\cos\theta_2$. On the contrary, the beam shift of the transmitted beam is on a downward trend as a whole with the optical thickness of the dielectric slab increasing. The beam shifts of the reflected and transmitted beams varying with the refractive index of the dielectric slab for $\theta_i = 30°$ and $H = \lambda_0/\cos\theta_2$ are presented in Fig. 11(b). It is clear that the beam shift of the reflected beam first increases and then decreases as the refractive index n_2 increasing. The maximum beam shift of the reflected beam is $1.2\lambda_0$ at $1.92 < n_2 < 2.26$. The variation trend of the beam shift of the transmitted beam with the refractive index of the dielectric slab is opposite to the beam shift of the reflected beam, and the beam shift has the maximum $-0.4\lambda_0$ at $1.12 < n_2 < 3.5$. Our results may give a new perspective for controlling the beam shift.

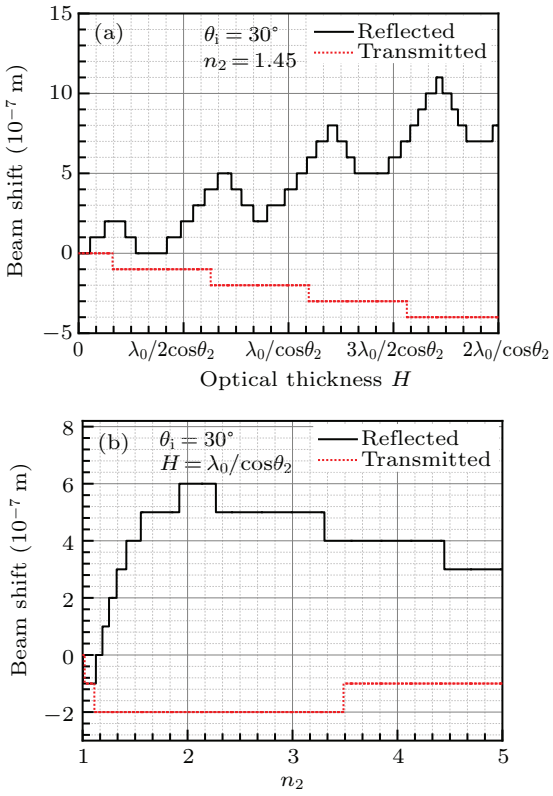


Fig. 11. Impinging at angle $\theta_i = 30°$, beam shifts of the reflected and transmitted beams as a function of (a) optical thickness H and (b) refractive index n_2 for the dielectric slab, respectively.

4. Conclusion

Based on the plane-wave angular spectrum expansion and Fresnel approximation, an analytical method have been proposed to study the reflection and transmission of a finite-power Airy beam incident in a dielectric slab. Through studying the intensity distributions of the reflected and transmitted beams at the refractive index of the dielectric slab $n_2 = 1$, the correctness of the method was verified. At $\theta_i = 30°$, the intensity distributions of the incident beam, reflected beam, internal beam as well as transmitted beam were simulated. Results showed that both the reflected and the transmitted beams are Airy-like shape and exhibit accelerating dynamics along the transverse direction, and the intensity of the transmitted beam is much greater than that of the reflected beam. Furthermore, the intensity distribution of each order beam mode field was also simulated. It was shown that the contribution of each order beam mode field to the actual beam field is related to the refractive index of the dielectric slab. In order to further study the interaction of Airy beam with the dielectric slab, the effects of the optical thickness and refractive index of the dielectric slab on the peak intensity and beam shifts of the reflected and transmitted beams were investigated. We found that the peak intensity of the reflected and transmitted beams varies periodically with the optical thickness of the dielectric slab, and the period is related to incident angle. Meanwhile, the variation of the peak intensity of the reflected and transmitted beams with the refractive index n_2 is different for different optical thicknesses and incident angles. The results in this paper may provide some theoretical supports to the design of optical films and the verification of numerical methods, and the analytical method can also be applied to the interaction of other focused beams such as Bessel beam and Hermite-Gaussian beam with layered media.

Acknowledgements

Project supported by the National Natural Science Foundation of China (Grant Nos. 62071359, 61975158, 62001377, and 61801349), China Postdoctoral Science Foundation (Grant No. 2016M602770), Natural Science Basic Research Plan in Shaanxi Province of China (Grant Nos. 2019JQ-405, 2019JM-238, 2020JM-192, and 2021JM-135), Natural Science Basic Research Program of Shaanxi, China (Grant No. 2020JQ-331), Postdoctoral Science Foundation in Shaanxi Province and the Fundamental Research Funds for the Central Universities, Scientific Research Program Funded by Shaanxi Provincial Education Department (Grant No. 20JS059), and the Open Foundation of Laboratory of Pinghu, Pinghu, China.

References

[1] Berry M V and Balazs N L 1979 *Am. J. Phys.* **47** 264
[2] Siviloglou G A, Broky J, Dogariu A and Christodoulides D N 2007 *Phys. Rev. Lett.* **99** 213901
[3] Siviloglou G A and Christodoulides D N 2007 *Opt. Lett.* **32** 979
[4] Siviloglou G A, Broky J, Dogariu A and Christodoulides D N 2008 *Opt. Lett.* **33** 207

[5] Efremidis N K, Chen Z, Segev M and Christodoulides D N 2019 *Optica* **6** 686

[6] Hu Y, Siviloglou G A, Zhang P, Efremidis N K, Christodoulides D N and Chen Z 2012 *Self-accelerating airy beams: Generation, control, and applications, Nonlinear photonics and novel optical phenomena* (New York: Springer)

[7] Baumgartl J, Mazilu M and Dholakia K 2008 *Nat. Photon.* **2** 675

[8] Zhang P, Prakash J, Zhang Z, Mills M S, Efremidis N K, Christodoulides D N and Chen Z 2011 *Opt. Lett.* **36** 2883

[9] Zheng Z, Zhang B F, Chen H, Ding J and Wang H T 2011 *Appl. Opt.* **50** 43

[10] Polynkin P, Kolesik M, Moloney J V, Siviloglou G A and Christodoulides D N 2009 *Science* **324** 229

[11] Polynkin P, Kolesik M and Moloney J 2009 *Phys. Rev. Lett.* **103** 123902

[12] Li J, Fan X, Zang W and Tian J 2011 *Opt. Lett.* **36** 648

[13] Li J, Zang W and Tian J 2010 *Opt. Express* **18** 7300

[14] Zhang P, Wang S, Liu Y, Yin X, Lu C, Chen Z and Zhang X 2011 *Opt. Lett.* **36** 3191

[15] Minovich A, Klein A E, Janunts N, Pertsch T, Neshev D N and Kivshar Y S 2011 *Phys. Rev. Lett.* **107** 116802

[16] Salandrino A and Christodoulides D N 2010 *Opt. Lett.* **35** 2082

[17] Li L, Li T, Wang S M, Zhang C and Zhu S N 2011 *Phys. Rev. Lett.* **107** 126804

[18] Liang Y, Hu Y, Song D, Lou C, Zhang X, Chen Z and Xu J 2015 *Opt. Lett.* **40** 5686

[19] Jia S, Vaughan J C and Zhuang X 2014 *Nat. Photon* **8** 302

[20] Vettenburg T, Dalgarno H I C, Nylk J, Coll-Lladó C, Ferrier D E K, Čižmár T, Gunn-Moore F J and Dholakia K 2014 *Nature Methods* **11** 541

[21] Born M and Wolf E, 1999 *Principles of optics* (Cambridge: Cambridge University Press)

[22] Goos V F and Hönchen H 1947 *Ann. Phys.* **436** 333

[23] Fedorov F I 1955 *Doklady Akademii Nauk SSSR* **105** 465

[24] Bliokh K Y and Aiello A 2013 *J. Opt.* **15** 014001

[25] Zhen W, Deng D and Guo J 2021 *Opt. Laser Techn.* **135** 106679

[26] Fan G and Deng D 2021 *Opt. Express* **29** 35182

[27] Lu Z, Zhen W, Wang G, Deng D and Guo J 2021 *Res. Phys.* **27** 104548

[28] Zhen W and Deng D 2020 *Appl. Phys. B* **126** 35

[29] Zhen W and Deng D 2020 *Opt. Commun.* **474** 126067

[30] Zhen W and Deng D 2020 *J. Phys. D: Appl. Phys.* **53** 255104

[31] Horowitz B R and Tamir T 1971 *J. Opt. Soc. Am. A* **61** 586

[32] Antar Y M and Boerner W M 1974 *Can. J. Phys.* **52** 962

[33] Okuda H and Sasada H 2008 *J. Opt. Soc. Am. A* **25** 881

[34] Ou J, Jiang Y, Zhang J and He Y 2013 *J. Opt. Soc. Am. A* **30** 2561

[35] Li H, Honary F, Wu Z and Bai L 2017 *J. Quant. Spectrosc. Radiat. Transf.* **195** 35

[36] Li H, Wu Z, Shang Q, Bai L and Li Z 2017 *Chin. Phys. B* **26** 034204

[37] Li H, Honary F, Wang J, Liu J, Wu Z and Bai L 2018 *Appl. Opt.* **57** 1967

[38] Wang M, Zhang H, Liu G, Li Y and Dong Q 2014 *Opt. Express* **22** 3705

[39] Yan B, Zhang H and Zhang J 2016 *Appl. Phys. B* **122** 174

[40] Li H, Liu J, Bai L and Wu Z 2018 *Appl. Opt.* **57** 7353

[41] Liu J W and Li H Y 2019 *Chin. Phys. B* **28** 094214

[42] Liu J, Li H, Li R, Bai L and Wu Z 2020 *J. Quant. Spectrosc. Radiat. Transf.* **251** 107046

[43] Chremmos I D and Efremidis N K 2012 *J. Opt. Soc. Am. A* **29** 861

[44] Efremidis N K 2014 *Phys. Rev. A* **89** 023841

[45] Li Y, Li L, Lu Y, Zhao X, Xu K, Zhang Y and Zhang Y 2013 *Opt. Express* **21** 8311

[46] Chamorro-Posada P, Sanchez-Curto J, Aceves A B and McDonald G S 2014 *Opt. Lett.* **39** 1378

[47] Zhen W and Deng D 2020 *Opt. Express* **28** 24104

[48] Gao M, Wang G, Yang X, Liu H and Deng D 2020 *Opt. Express* **28** 28916

[49] Gao M and Deng D 2020 *Opt. Express* **28** 10531

[50] Ornigotti M 2018 *Opt. Lett.* **43** 1411

[51] Kong J A, Wu B I and Zhang Y 2002 *Microw. Opt. Technol. Lett.* **33** 136

[52] Chew W C 1995 *Waves and fields in inhomogeneous media* (New York: IEEE press)

[53] Read L A A, Wong M and Reesor G E 1978 *J. Opt. Soc. Am. A* **68** 319